Int. J. Electrochem. Sci., 13 **(2018)** 3501 – 3515, doi: 10.20964/2018.04.31

International Journal of
ELECTROCHEMICAL
SCIENCE
www.electrochemsci.org

Synergetic Optimization via Composition-Dependent Nanostructuring in Co-Mo-S Electrocatalysts for Efficient Hydrogen Evolution in Alkaline Solution

Bo Wang[1], *Yanhong Liu*[*,1], *Jinhui Hao*[1], *Junbo Zhong*[2], *Furong Yu*[1], *Kewei Zhang*[1], *Hao Shen*[*,1] *and Baodong Mao*[*,1]

[1] School of Chemistry and Chemical Engineering, Jiangsu University, Zhenjiang 212013, P.R. China
[2] Key Laboratory of Green Catalysis of Higher Education Institutes of Sichuan, College of Chemistry and Environmental Engineering, Sichuan University of Science and Engineering, Zigong 643000, P.R. China
[*]E-mail: liuyh@ujs.edu.cn, ujsshenhao@163.com, maobd@ujs.edu.cn

Received: 10 January 2018 / *Accepted:* 6 February 2018 / *Published:* 6 March 2018

Earth-abundant metal sulfides attracts large attention in recent years for hydrogen production via electrocatalytic water splitting. However, most works have been limited to the acidic condition, whereas the hydrogen evolution reaction (HER) in alkaline condition has rarely been discussed. Here we present an effective strategy for the growing of Co-Mo-S catalysts on carbon cloth via the controllable incorporation of cobalt into MoS_2 with L-cysteine and phosphomolybdic acid to achieve the synergistic interaction of CoS_2 and MoS_2. The optimized Co-Mo-S catalysts (Co:Mo=1:2) showed a largely improved HER activity with an overpotential of 92 mV at current density of 10 mA cm^{-2} and Tafel slope of 82 mV dec^{-1}. The origin of the activity enhancement was investigated through a series of characterizations, where the synergetic effect of the intrinsic fast HER kinetics of metallic CoS_2 and the high active surface area of MoS_2 plays a crucial role. With appropriate amount of cobalt, the Co-Mo-S catalysts show a relatively uniform distribution on the carbon cloth to ensure the large surface area, whereas excessive cobalt results in the formation of the large CoS_2 particles with low HER activity from the low active surface area. Further electrochemical measurements demonstrated that the combination of larger exchange current density of CoS_2 and the high electrochemical double–layer capacitance (proportional to the active surface area) of MoS_2 together contributed to the HER activity enhancement of the Co-Mo-S catalysts. The Co-Mo-S/CC catalysts also show robust stability in alkaline solution. Our work provides a more profound understanding and an interesting view for the design of efficient ternary transition metal sulfide HER catalysts in alkaline condition by synergetic optimization of the intrinsic HER kinetics and the electrochemical active surface area.

Keywords: molybdenum sulfide; cobalt sulfide; carbon cloth; hydrogen evolution reaction; alkaline solution

1. INTRODUCTION

Driven by rapid depletion of fossil fuels and increasing global warming issues, finding renewable and clean energy is extremely urgent [1, 2]. Hydrogen, as an ideal green energy, possesses the highest gravimetric energy density and no pollution which burned was only water [3]. Hydrogen production from electrocatalytic water splitting is becoming more and more important for renewable energy applications [4, 5]. Noble metals such as Pt represents the most effective catalysts, for which the high cost and scarcity nature greatly hinder their widespread applications [6]. Tremendous efforts have been contributed to the development of cost-effective electrocatalysts based on earth-abundant elements, such as transition metal sulphides [7-10], phosphides [11-15], and carbides [16-19] with high activity and stability. On the other hand, alkaline water electrolysis is important for industrial applications. However, even the catalytic activity of Pt is about two orders of magnitude lower than that in acidic electrolytes [20]. It is of great interest to develop cost-effective electrocatalysts based on inexpensive and earth abundant elements for hydrogen evolution reaction (HER) in alkaline environment [16, 21-23].

Transition metal sulfides, as low-cost alternatives, show great promise for alkaline water electrolysis. As demonstrated in acidic HER, ternary metal sulfides including two types of transition metal ions show high activity due to the enhanced intrinsic activity and the fast charge transport because of the synergistic effects of different elements [15, 24-29]. Although the effect of transition metal doped MoSx has been well studied, the reports on mechanism and structure tuning study are much less for alkaline HER. For HER in alkali, an important consideration is the simultaneous optimization of the activity and stability. Markovic et al. reported the CoMoSx chalcogel structure by combining the high activity of CoS_2 building blocks with the high stability of MoSx units into a composite to design an efficient HER electrocatalyst in both alkaline and acidic environments [30]. After that, a few works have been contributed to the structure regulation of transition metal-doped MoS_2 electrocatalysts for HER in alkali. Yan et al. have prepared hollow chevrel-phase $NiMo_3S_4$ by a template-directed anion exchange method, which show good HER performance and remarkable robustness in alkali [31]. Recently, porous CoMoS nanosheets with a defect-rich structure have been reported with largely improved HER performance compared to single CoS_2 and MoS_2 [32]. Interlaced NiS_2-MoS_2 nanoflake-nanowires were anchored on titanium foils by a two-step method to achieve excellent HER catalytic activity [33]. It is of great interest to further explore the structure tuning of the low-cost metal sulfides for alkaline HER towards a sustainable future.

Here, we report a simple strategy for the growing and optimization of Co-Mo-S HER catalysts on carbon cloth (denoted as Co-Mo-S/CC) via the controllable incorporation of cobalt into MoS_2 with an L-cysteine-assisted hydrothermal method (Scheme 1). Much superior HER activity were observed in the Co-Mo-S catalysts compared to the single components (MoS_2 or CoS_2) under alkaline condition. The activity of the Co-Mo-S catalysts was optimized by simply varying the Co/Mo ratio, for which morphological effect plays an important role. It was observed that the synergetic effect was achieved through the compromise of the intrinsic fast HER kinetics of CoS_2 and the high surface area of MoS_2. As a proof-of-concept, the Co-Mo-S/CC electrocatalyst exhibits an excelent HER activity in alkali with low onset potential of 34 mV, an overpotential of 92 mV to reach a current density of 10 mA cm^{-2}, a small Tafel slope (82 mV dec^{-1}), and it also offers excellent stability.

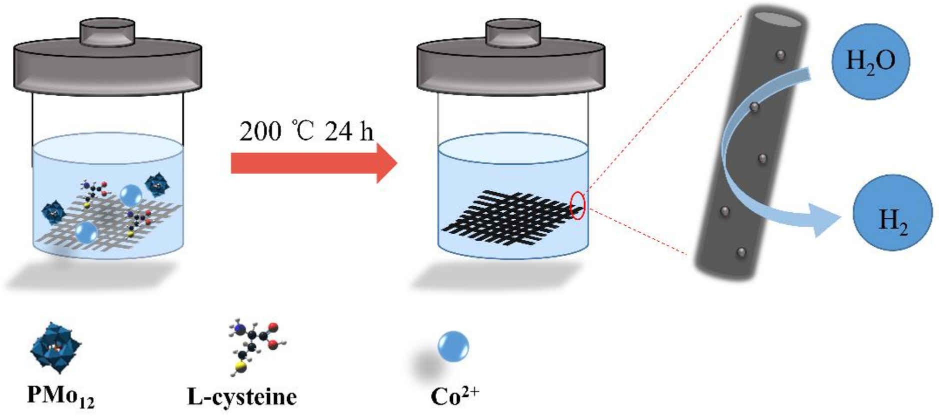

Scheme 1. Schematic illustration for the preparation of the Co-Mo-S catalysts on carbon cloth.

2. EXPERIMENTAL SECTION

2.1 Reagents and materials

All chemicals are analytically pure and used without further purification. Carbon cloth (CC) was bought from Hesenbio Ltd. (Shanghai, China). Phosphomolybdic acid ($H_3PMo_{12}O_{40}\cdot xH_2O$, PMo_{12}) was purchased from Sinopharm Chemical Reagent Co. Ltd. L-cysteine (99.5%), cobalt nitrate ($Co(NO_3)_2\cdot 6H_2O$) and potassium hydroxide (KOH) were purchased from Aladdin (China). Graphite rod (99.9995%) was purchased from Sigma-Aldrich. The water used in the experiments was ultra-pure water.

2.2 Preparation of MoS_2, CoS_2 and Co-Mo-S on carbon cloth

Firstly, carbon cloth was sonicated with acetone, ethanol and deionized water several times to clean the surface before use. In brief, certain amount of cobalt nitrate and phosphomolybdic acid were used as Co and Mo sources with different ratios (Co and Mo sum of 2 mmol), where L-cysteine (4.3 mmol) aqueous solution (30 mL) was added as both the S source and the reducing agent to form a homogeneous solution. The solution with a piece of CC (1×2 cm^2) was transferred into a 50 mL Teflon-lined stainless steel autoclave and maintained at 200 °C for 24 h, which was then cooled down to room temperature naturally. The final products (denoted as Co-Mo-S(1:x)/CC, x=1, 2, 3, and 1:x as the molar ratio of Co:Mo) were washed with deionized water and absolute ethanol, and dried in a vacuum oven at 60 °C overnight.

Similarly, MoS_2/CC and CoS_2/CC were obtained with the same method. MoS_2/CC was prepared using 0.167 mmol PMo_{12} and 4.3 mmol L-cysteine, and CoS_2/CC was prepared used 2 mmol cobalt nitrate and 4.3 mmol L-cysteine as the precursors at 200 °C for 24 h, respectively.

2.3 Characterization

Crystal structure of the samples were studied by X-ray diffraction (XRD) using Cu-Kα radiation source (λ= 1.54056 Å) under 40 kV and 40 mA ranging from 5° to 75° at a scanning rate of 5.0° min^{-1} (Bruker AXS, Germany). Raman spectra were recorded with an America ThermoFisher (DXR) Laser Raman Spectrometer with a 532 nm laser. The morphology of the samples was observed using a field emission scanning electron microscope (FESEM, Hitachi S-4800, Japan). Transmission electron microscopy (TEM), high-resolution TEM (HRTEM) and scanning transmission electron microscopy (STEM) were also used to explore the structure of the samples with a Tecnai G2 F30 S-Twin (FEI) electron microscope with an accelerating voltage of 200 kV. The X-ray photoelectron spectra (XPS) were obtained using an ESCALAB 250X (Thermo Fisher Scientifc, USA) electron spectrometer with 150 W Al Kα X-ray sources.

2.4 Electrochemical measurements

Electrochemical measurements were performed at room temperature with a CHI 760E electrochemical workstation. A typical three-electrode cell was used, in which the samples were used as the working electrode, a saturated calomel electrode (SCE) as the reference electrode, and a graphite rod as the counter electrode. In all measurements, the SCE reference electrode was calibrated with respect to the reversible hydrogen electrode (RHE), where E(RHE)= E(SCE) + 1.058V in 1.0 M potassium hydroxide (KOH, pH=13.8). The electrochemical measurement was performed with N_2-saturated electrolyte.

Linear sweep voltammetry (LSV) was performed in different electrolyte solutions with the scan rate of 5 mV s^{-1}. Cyclic voltammetry (CV) was conducted at the scan rates of 20, 40, 60, 80 and 100 mV s^{-1} in the potential rang of 0.1 to 0.2 V for the investigation of electrochemical double-layer capacitances (C_{dl}). For stability test, CV was performed for 1000 cycles with a scan rate of 100 mV s^{-1} in the potential range from −0.15 to 0.1 V. The amperometric i−t curves were obtained at a static overpotential of 92 mV. Electrochemical impedance spectroscopy (EIS) measurements were conducted under an overpotential of 140 mV with frequency ranging from 100 kHz to 0.01 Hz with an AC voltage of 5 mV. In order to reflect the actual catalytic currents, all polarization curves were corrected with the iR compensation.

3. RESULTS AND DISCUSSION

3.1. Characterisation of Co-Mo-S/CC nanocomposities

In the synthetic strategy, Co^{2+} was introduced into MoS_2 to adjust the morphologies and to improve the intrinsic activities of MoS_2. Fig. 1 shows the SEM images of bare CC, MoS_2/CC, Co-Mo-S(1:3)/CC, Co-Mo-S(1:2)/CC, Co-Mo-S(1:1)/CC and CoS_2/CC. Fig. 1b showed the morphology of the as-prepared MoS_2/CC, where the surface of carbon cloth was uniformly covered with MoS_2 with few amount aggregates. The introduction of few Co^{2+} into the precursor solution played a critical role in tuning the nanostructure of Co-Mo-S/CC. As shown in Fig. 1c and 1d, with the Co to Mo molar ratio of 1:3 and 1:2, the relatively uniform Co-Mo-S nanoparticles (~50-100 nm) was well-distributed, on the surface of carbon fibers, simultaneously. Moreover, with further increase of Co:Mo ratio to 1:1 (Fig. 1e) and 2:0 (pure CoS_2, Fig. 1f), the surface of carbon fibers emerge massive peanut-like particles with sizes ranging from 500 nm to 2 μm.

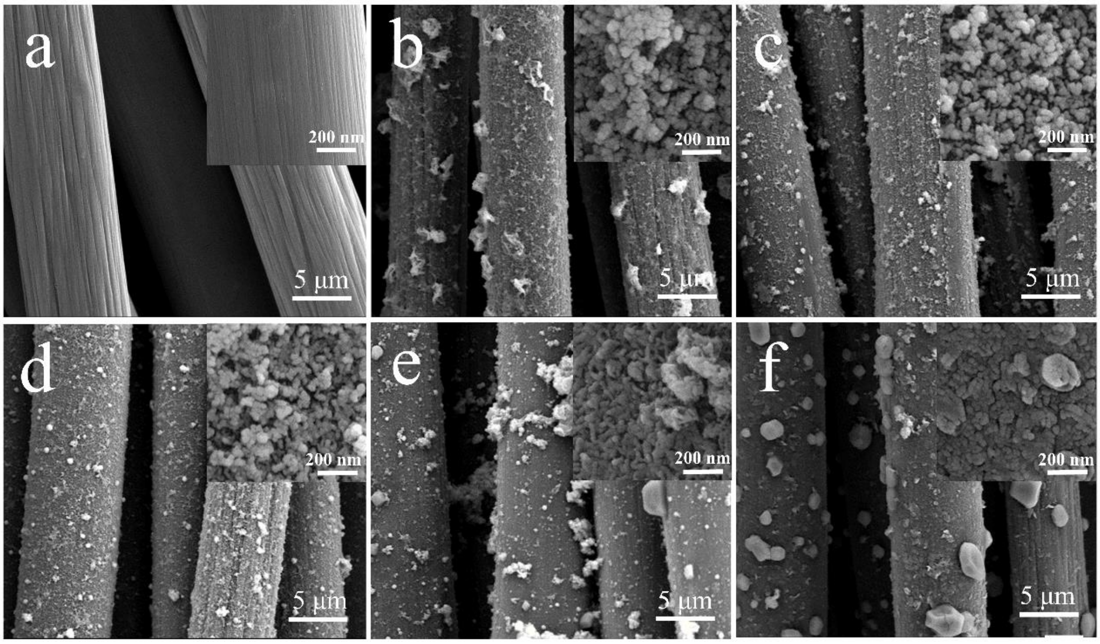

Figure 1. Low-resolution SEM images of (a) bare CC, (b) MoS_2/CC, (c) Co-Mo-S(1:3)/CC, Co-Mo-S(1:2)/CC (d), Co-Mo-S(1:1)/CC (e) and CoS_2/CC (f), Insets: high magnification SEM images.

To better elucidate the microscopic structure of Co-Mo-S(1:2)/CC, the Co-Mo-S composites were further peeled off from the carbon cloth by sonication and investigated by TEM. As shown in Fig. 2a, the introduction of Co^{2+} during the synthesis formed the porous hybrid Co-Mo-S structure. HRTEM image (Fig. 2b) indicates the formation of intimate contacts of CoS_2 and MoS_2 in the Co-Mo-S hybrid. The lattice with spacing of 0.241 nm and 0.277 nm are assigned to the (210) and (200) crystal planes of pyrite phase CoS_2 [34]. Furthermore, the lattice planes with a spacing of 0.27 nm can be indexed into the (110) crystal plane of 2H-MoS_2, though it is not easy to be distinguished from the CoS_2 (200) plane. Moreover, the spacing of ~0.92 nm between two adjacent monolayers, further demonstrates the existence of the MoS_2 (002) planes with expanded interlayer spacing, which is much larger than that of the pristine MoS_2 of ~0.65 nm, that may come from the introduction of Co^{2+} into the basal plane of Co-Mo-S. EDS mapping was performed to further demonstrate the existence of these elements. Fig. 2c shows that the Co, Mo and S elements were distributed homogeneously in the optimized Co-Mo-S(1:2) sample.

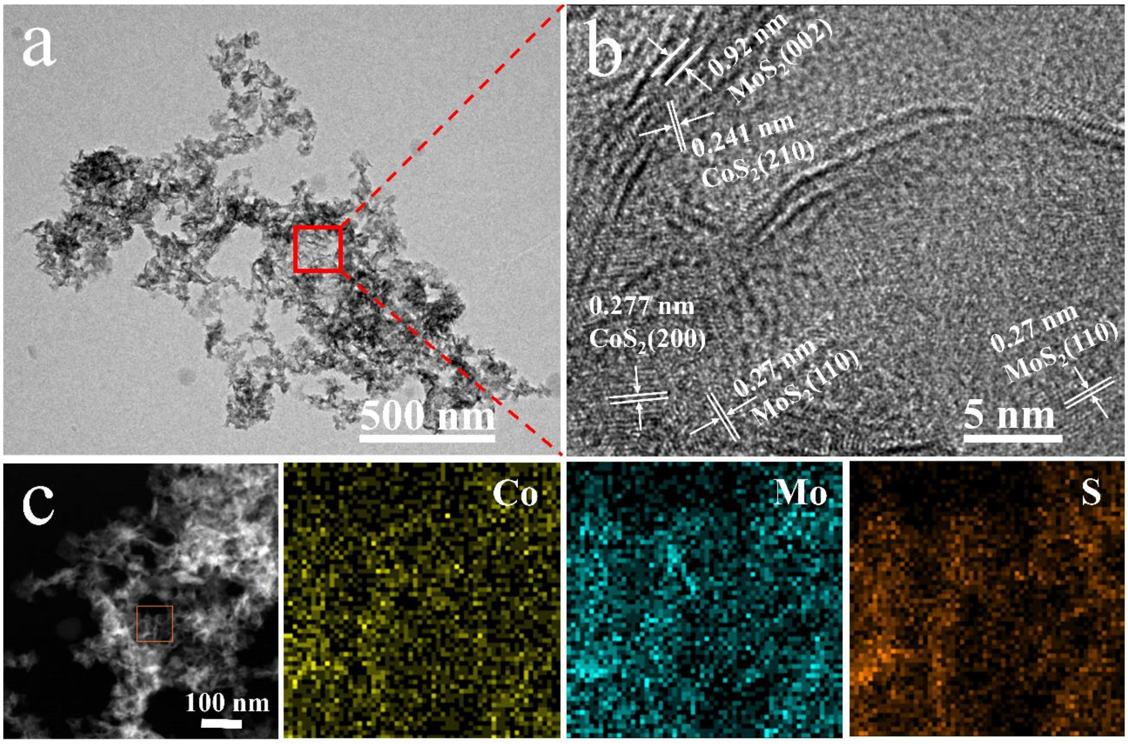

Figure 2. Low-magnification TEM image (a), HRTEM image (b) and elemental mapping (c) of the Co-Mo-S(1:2)/CC sample.

XRD was used to investigate the crystal structure of Co-Mo-S samples. As shown in Fig. 3a, the strong diffraction peak at 26° was assigned to the carbon cloth substrate (red line, Co-Mo-S(1:2)/CC). The diffraction peaks at 43.2° can be indexed to the (006) plane of the hexagonal phase 2H-MoS$_2$ (JCPDF# 87-2416) [35, 36]. However, due to the strong interference of carbon cloth, XRD peaks of Co-Mo-S were not clearly demonstrated. Further, XRD measurement was performed after peeled off from carbon fiber. The two diffraction peaks centered at around 32.5° and 55.2°, can be assigned to the (210) and (200) crystal planes of pyrite phase CoS$_2$ (JCPDF# 70-2865), respectively. The diffraction peaks at 24°, 43.2°, and 58.7° can be well indexed to the (100), (006) and (110) planes of the hexagonal 2H-MoS$_2$, indicating the coexistence of cobalt and molybdenum elements in Co-Mo-S/CC [34, 37]. In addition, a new diffraction peak appeared at 9.8°, corresponding to the shift (002) plane of MoS$_2$, which suggests that the introduction of Co^{2+} enlarged the interlayer spacing in Co-Mo-S which can lead to high activity for HER. In this case, the spacing between two adjacent layers can be calculated using Bragg's law $n\lambda = 2d\sin\theta$ [38], where n is the order of reflection, λ is the wavelength of the incident X-ray, d is the interlayer spacing and θ is the angle between the incident X-ray and the scattering planes. The calculated spacing between Mo-S layers was about 0.92 nm which is consistent with the observation in HRTEM. Raman spectrum was further measured to identify the structure of the as-obtained sample. As show in Fig. 3b, Co-Mo-S(1:2)/CC displays a peak at 390 cm^{-1}, corresponding to the in-phase stretch (A_g) mode of CoS$_2$ [39]. Moreover, the distinct peak at ~380 cm^{-1} associated to the in-plane E_{2g}^{1} mode and two distinct peaks at ~403 and ~410 cm^{-1} are associated to the out-of-plane A_{1g} vibration modes of the hexagonal 2H-MoS$_2$ [34, 40, 41].

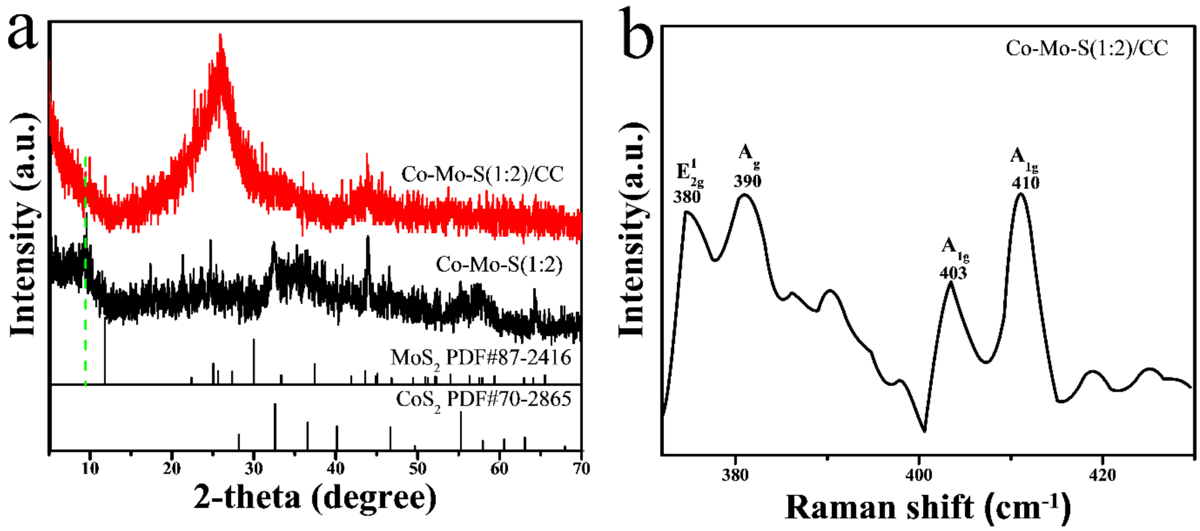

Figure 3. (a) XRD patterns of Co-Mo-S(1:2)/CC and the peeled off Co-Mo-S(1:2) samples, and (b) Raman spectra of Co-Mo-S(1:2)/CC.

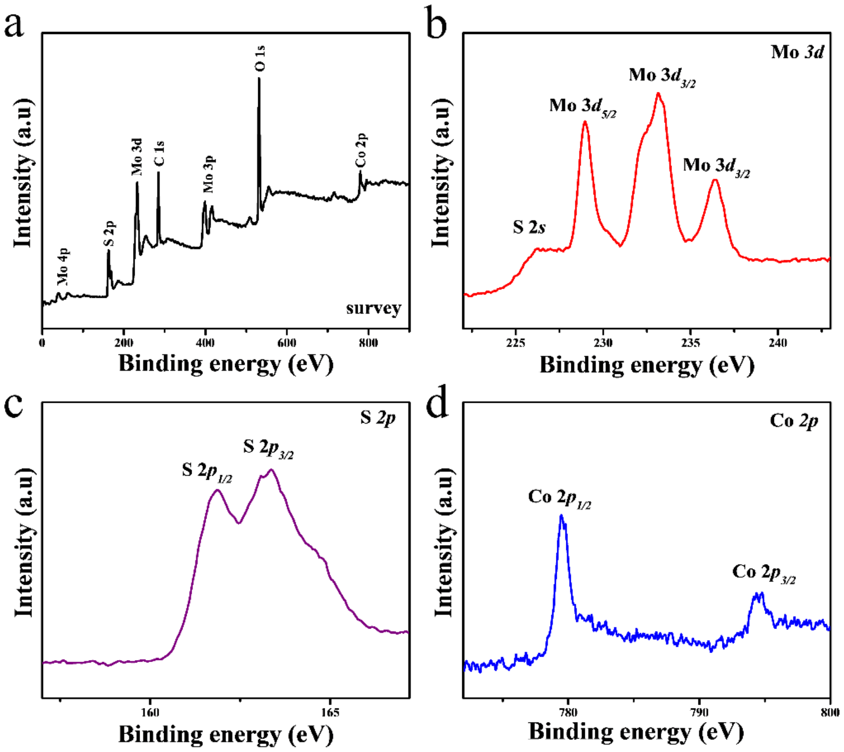

Figure 4. XPS spectra of Co-Mo-S(1:2)/CC: (a) survey, (b) Mo 3d, (c) S 2p, and (d) Co 2p.

XPS was used to examine the chemical composition and chemical element states of Co-Mo-S(1:2)/CC. The survey spectrum recorded from 0 to 900 eV in Fig. 4a confirms the presence of Co, Mo, S, C and O elements. From the high- resolution XPS spectrum of Mo 3d (Fig. 4b), two major peaks at 228.9 and 233 eV were observed and can be assigned to the characteristic doublet peaks of Mo^{4+} $3d_{5/2}$ and $3d_{3/2}$ core electrons [42, 43]. In addition, the characteristic peak at 236 eV correspond to Mo-O bond, which may be due to the inadequate reduction of MoO_4^{2-} during the hydrothermal process [44, 45]. Moreover, a small peak appears at 226.6 eV that can be ascribed to the S 2s orbital. The peaks at 161.9 and 163.3 eV can be assigned to the S $2p_{1/2}$ and $2p_{3/2}$ orbitals, indicating the -2 oxidation state of sulfur in MoS_2 (Fig. 4c) [44]. Fig. 4d showed the Co 2p spectrum, two peaks can be assigned to Co $2p_{3/2}$ and Co $2p_{1/2}$ at 779.5 and 795.4 eV, respectively. It is worth to note that the intensity of Co spectrum was lower than other elements, which may be attributed to its lower content in the Co-Mo-S (1:2)/CC sample.

3.2. Electrocatalytic activity of Co-Mo-S/CC toward HER

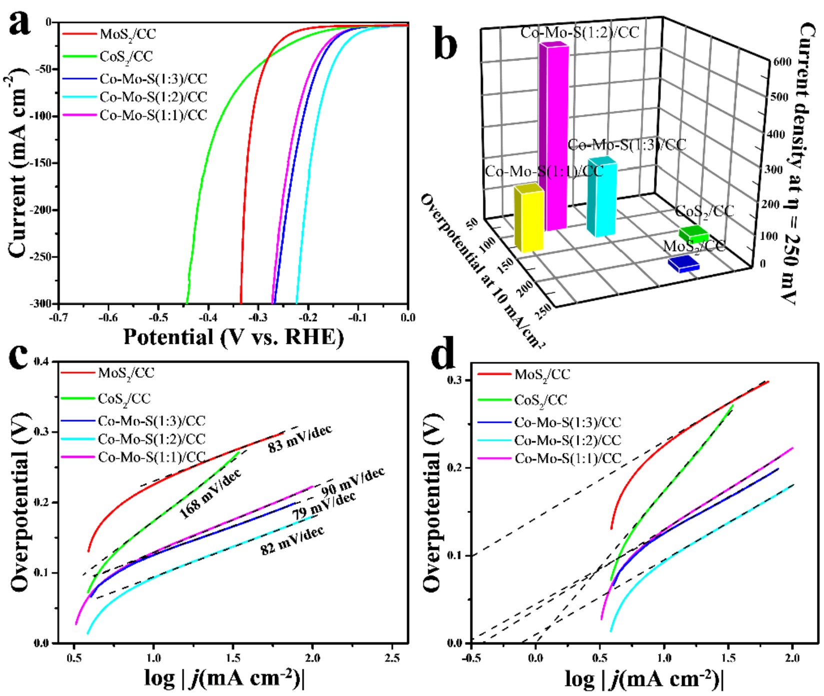

Figure 5. (a) HER polarization curves and (b) HER performance comparison (η_{10} and current densities at η = 250 mV) of MoS_2/CC, CoS_2/CC, Co-Mo-S(1:3)/CC, Co-Mo-S(1:2)/CC, and Co-Mo-S(1:1)/CC. (c) Corresponding Tafel slopes obtained from panel (a). (d) Calculated exchange current densities of MoS_2/CC, CoS_2/CC, Co-Mo-S(1:3)/CC, Co-Mo-S(1:2)/CC, and Co-Mo-S(1:1)/CC by applying extrapolation method to the Tafel plots.

To investigate the HER activities of the Co-Mo-S catalysts, electrochemical measurements were carried out using a standard three-electrode cell in N_2-saturated 1 M KOH solution. All of the samples were grown on carbon cloth and were used directly as working electrodes without other treatment. For comparison, the catalytic activities of MoS_2/CC and CoS_2/CC were also examined with the same setup. As shown in Fig. 5a, the HER onset potentials of CoS_2/CC is approximately 85 mV, substantially lower than that of MoS_2/CC (ca. 151 mV), suggesting that CoS_2 material is intrinsically more active than MoS_2 [30]. When Co was introduced into MoS_2 (Co:Mo = 1:3), the HER performance of Co-Mo-S catalysts significantly was significantly enhanced and achieved maximum with Co:Mo ratio of 1:2 (onset potential of 34 mV), indicating the important role of Co to improve the electrocatalytic activity of MoS_2. However, further increase of Co:Mo ratio of 1:1 resulted in the increase of the onset potential (53 mV). Among all the studied samples, Co-Mo-S(1:2)/CC shows the best catalytic activity for HER in alkaline electrolyte with a lower overpotential (92 mV) at the current density of 10 mA cm^{-2}, substantially lower than of CoS_2/CC (173 mV) and MoS_2/CC (224 mV), which also outperforms most of the transition metal sulfides electrocatalysts for alkaline HER (Table 1), including defect-rich CoMoS [46], MoS_2/Ni_3S_2 heterostructures [47], and MoS_2/Mo [48]. Moreover, the current density at η = 250 mV of Co-Mo-S(1:2)/CC reaches 570 mA cm^{-2}, which is 21 and 33.5 times than that of CoS_2/CC and MoS_2/CC, respectively, indicating the largely improved HER activity of Co-Mo-S/CC (Fig. 5b).

Table 1. Comparison of HER performance in 1M KOH for Co-Mo-S/CC with reported electrocatalysts.

Catalysts	Electrolyte solution	η_{onset} (mV)	η_{10} (mV)	Tafel slope (mV dec^{-1})	Reference
Co-Mo-S/CC	1M KOH	34	92	82	This work
Chevrel-phase $NiMo_3S_4$	0.1M KOH	59	257	98	[31]
Defect-rich CoMoS	1M KOH	42	98	82	[46]
MoS_2/Ni_3S_2 heterostructures	1M KOH	50	110	88	[47]
MoS_2 nanosheets		236	431	308	
MoS_2/Mo	1M KOH	---	184	87	[48]
Cu@CoS_x/CF	1M KOH	95	134	61	[49]
Ni_3S_2/nickel foam	1M KOH	59	223	---	[50]

Table 2. Summary of HER activity of Co-Mo-S(1:3)/CC, Co-Mo-S(1:2)/CC, Co-Mo-S(1:1)/CC, CoS_2/CC and MoS_2/CC in 1 M KOH.

Catalysts	η_{onset} (mV)	η_{10} (mV)	Tafel slope (mV dec^{-1})	j_0 (mA cm^{-2})	R_{ct} (Ω)
MoS_2/CC	151	224	83	1.39×10^{-2}	582
CoS_2/CC	85	173	168	9.89×10^{-1}	260
Co-Mo-S(1:3)/CC	60	124	79	2.87×10^{-1}	36
Co-Mo-S(1:2)/CC	34	92	82	7.82×10^{-1}	29
Co-Mo-S(1:1)/CC	53	130	90	3.92×10^{-1}	83

To assess the intrinsic HER activities of the catalysts, Tafel slopes were obtained according to the Tafel equation ($\eta = b\log j + a$), where η, b, j and a are the overpotential, Tafel slope, current density, and a constant, respectively [51-54]. As shown in Fig. 5c, the Tafel slopes were 79, 82, 90, 168 and 83 mV dec^{-1} for Co-Mo-S(1:3)/CC, Co-Mo-S(1:2)/CC, Co-Mo-S(1:1)/CC, CoS_2/CC and MoS_2/CC, respectively. The Tafel slope of Co-Mo-S(1:2)/CC is much lower than CoS_2/CC and MoS_2/CC, suggesting a combined Volmer-Heyrovsky mechanism for HER [35]. Exchange current density (j_0) reflects the intrinsic catalytic efficiency of electrocatalysts, which can be calculated by extrapolating the Tafel plots to the x axis. The j_0 can be obtained by assuming η was zero with the Tafel equation

[55]. As shown in Fig 5d, the j_0 value of Co-Mo-S(1:2)/CC was 56 times larger than that of MoS_2/CC (Table 2). The high exchange current density reveals the origin of the excellent HER activity of the Co-Mo-S/CC samples. It worth to mention that CoS_2 actually shows the highest exchange current density and also shows a low onset potential of 85 mV, indicating its high intrinsic activity plays a crucial role in the activity enhancement of Co-Mo-S [30].

To better understand the effect Co incorporation, the electrochemical double–layer capacitance (C_{dl}) was further used to estimate the effective surface areas by CV tests in the 0.1–0.2 V region as shown in Fig 6 [45, 56-58]. As shown in Fig. 6d, the values of C_{dl} are 107, 88.2 and 2.8 mF cm^{-2} for Co-Mo-S(1:2)/CC, MoS_2/CC and CoS_2/CC, indicating the hybrid Co-Mo-S(1:2)/CC possess the highest effective surface area for HER. The value of C_{dl} for MoS_2/CC was much larger than that of CoS_2/CC and close to that of Co-Mo-S(1:2)/CC, which suggests that MoS_2 plays a main role in the enlarged surface area of Co-Mo-S with appropriate amount of Co. This also explains the activity loss with the extra Co that forms large particles as shown in Fig 1e, which results in the low active surface area decrease the HER activity.

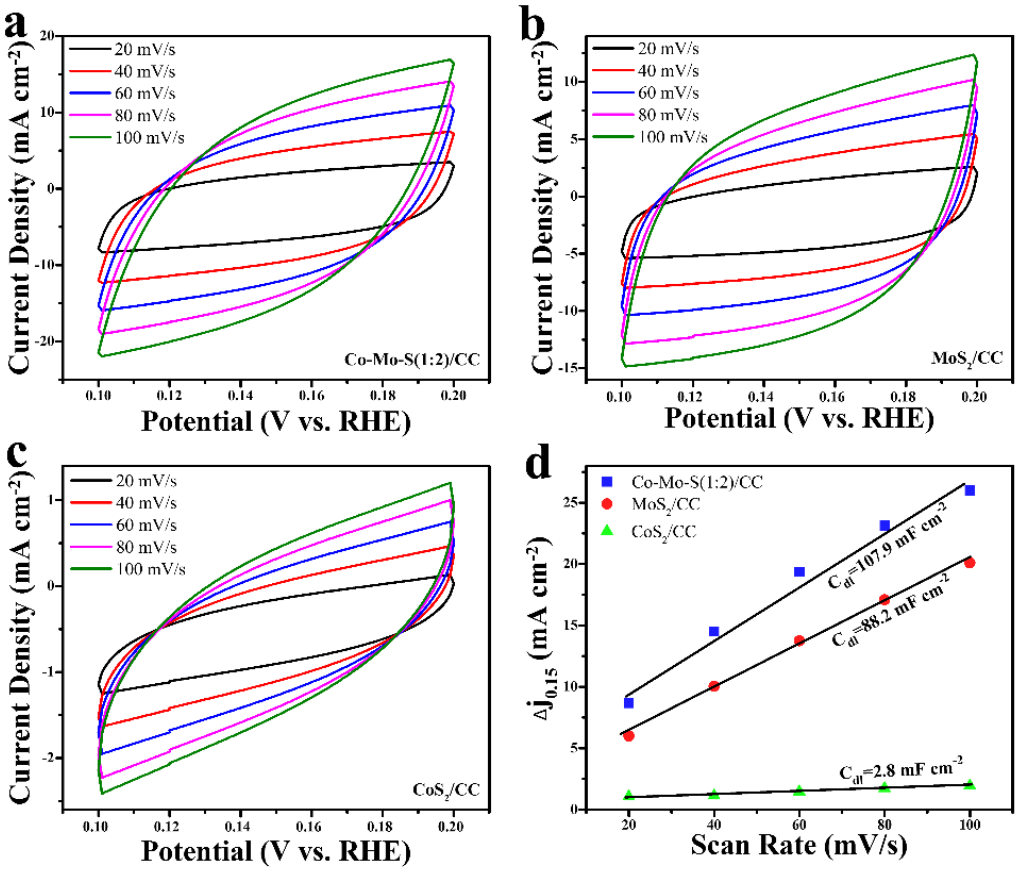

Figure 6. CV curves of (a) Co-Mo-S(1:2)/CC, (b) MoS_2/CC and (c) CoS_2/CC measured from 20 to 100 mV s^{-1}, and (d) the capacitive currents (Δj) at 0.15 V vs RHE plotted as a function of scan rate from which Cdl was calculated by linear fitting.

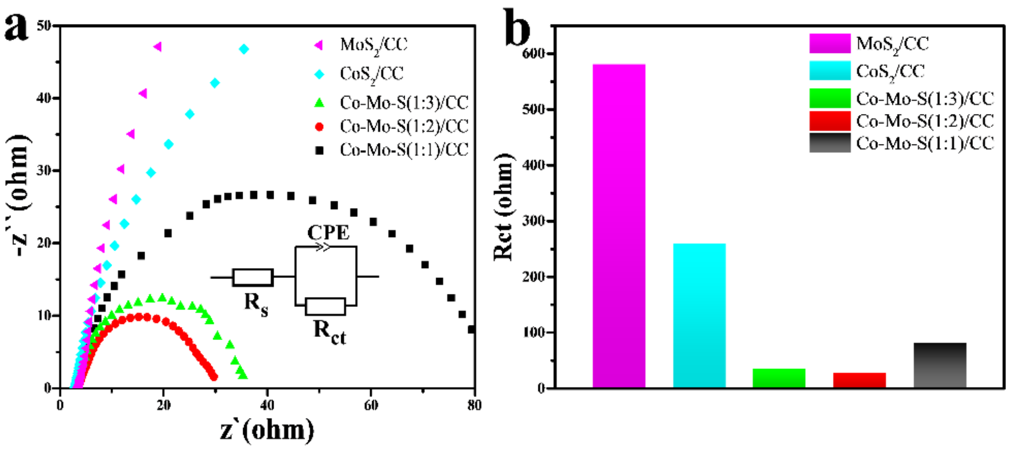

Figure 7. (a) Nyquist plots of MoS_2/CC, CoS_2/CC, Co-Mo-S(1:3)/CC, Co-Mo-S(1:2)/CC, and Co-Mo-S(1:1)/CC. (b) Plot of charge transport resistance of different samples.

The electrochemical impedances of Co-Mo-S/CC were measured by EIS measurement to investigate the HER kinetics at the interface between the electrode and electrolyte [59, 60]. As shown in Fig. 7a, the fitted results reveal that the Co-Mo-S(1:2)/CC shows the smallest charge-transfer resistance (R_{ct}) than others, indicating a faster Faradaic process in HER kinetics. It worth to mention that, the value of R_{ct} for CoS_2/CC is smaller than MoS_2/CC, indicating CoS_2/CC possess faster charge transfer. The R_{ct} values summarized Fig. 6b show the same tendency with the HER overpotential tests (Fig. 5a), where the charge transfer efficiency is largely improved in the Co-Mo-S catalysts compared to single MoS_2 and CoS_2.

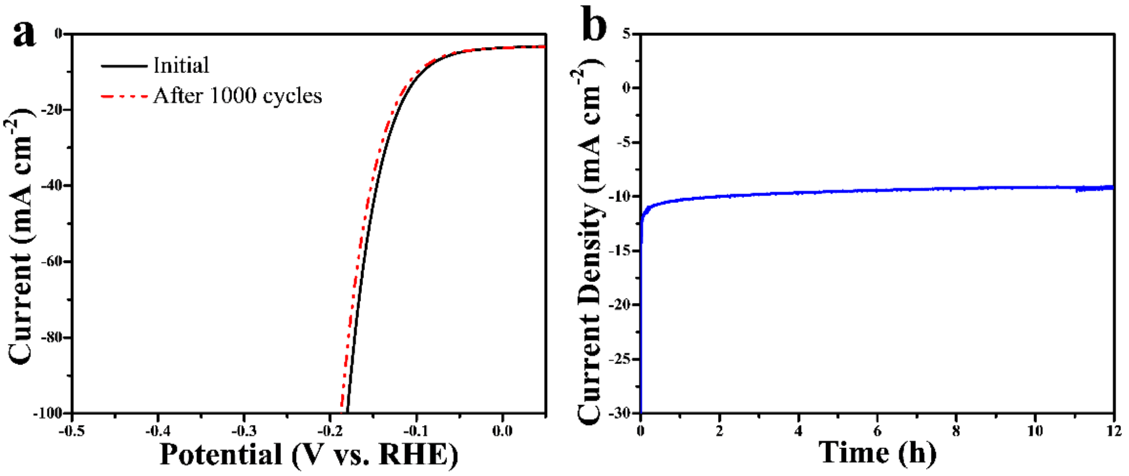

Figure 8. (a) Durability measurement of Co-Mo-S(1:2)/CC. The solid line and dotted lines are the polarization curves recorded initially and after 1000 cycles (scan rate: 100 mV s^{-1}), respectively. (b) Time-depentent current density of Co-Mo-S(1:2)/CC under a static overpotential of 92 mV.

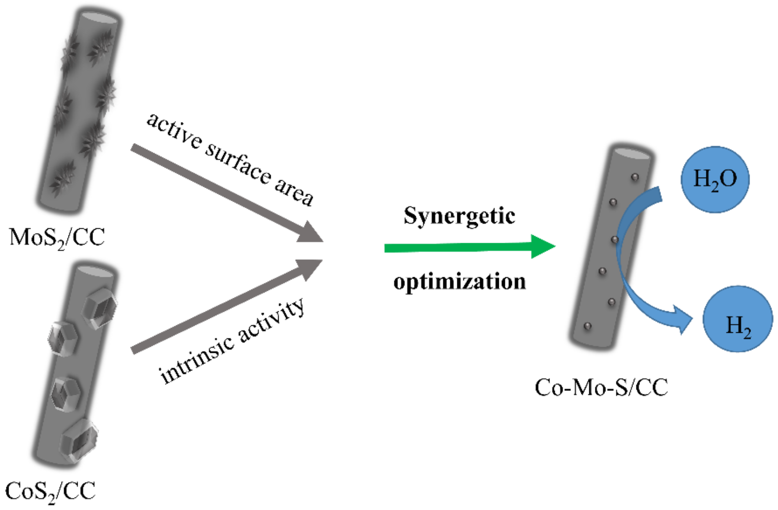

Scheme 2. Schematic illustration for the synergetic optimization of the Co-Mo-S/CC catalysts employing the high active surface area of MoS_2 and the high intrinsic activity of CoS_2.

We further evaluated the stability and durability of the Co-Mo-S(1:2)/CC catalyst by continuous CV sweeping from -0.15 to 0.1 V at a scan rate of 100 mV s^{-1}. As shown in Fig. 8a, after 1000 cycles, the current loss is negligible in the polarization curve of Co-Mo-S(1:2)/CC. The long-term durability was conducted around ~10 mA cm^{-2} of this catalyst by a continuous current measurement at 92 mV in 1 M KOH solution (Fig. 8b). After 12 hours of continuous test, the Co-Mo-S(1:2)/CC still remain 91% of its original current density, suggests that the robust stability for HER in strong alkaline electrolyte.

Based on the above results, the superior alkaline HER activity and stability of the Co-Mo-S/CC can be ascribed to the following aspects, as a result of the synergetic effect of CoS_2 and MoS_2 as shown in Scheme 2. (1) CC acts as a good current collector, which can enhance the charge transport of the composite material [61]; (2) Metallic CoS_2 possess the fast intrinsic HER kinetics, where the semiconducting MoS_2 have higher effective surface area, from which the synergetic effect of CoS_2 and MoS_2 are possible to achieve an enhanced activity [30]; (3) The incorporation of appropriate amount of cobalt is crucial to avoid the formation of large CoS_2 particles and ensure the high active surface area and relatively uniform distribution of the Co-Mo-S catalysts on the carbon cloth, which enables the high activity [44]. Our result provides an important guideline for the design of the transition metal doped MoS_2 electrocatalysts for efficient alkaline HER by composition-dependent nanostructuring, which may be of great interest for industrial water electrolyzers.

4. CONCLUSIONS

In summary, we have developed an effective strategy for the growing of Co-Mo-S catalysts on carbon cloth (CC) via introducing cobalt into MoS_2 to achieve the synergistic interaction of CoS_2 and MoS_2 and demonstrated to be efficient HER catalysts in alkaline condition. The optimized Co-Mo-S catalysts (Co:Mo=1:2) showed a largely improved HER activity with an overpotential of 92 mV at a current density of 10 mA cm^{-2} and Tafel slope of 82 mV dec^{-1}. The Co-Mo-S catalysts also show good stability for alkaline HER. The enhanced activity and stability of Co-Mo-S/CC are ascribed to the synergistic effect of fast intrinsic HER kinetics of metallic CoS_2 and high effective surface area and abundant active sites of semiconducting MoS_2. Our results indicated that one of the most important consideration is the incorporation of appropriate amount of Co into MoS_2 to avoid the overgrowth of large CoS_2 particles and maintain the high surface area of Co-Mo-S nanostructures. This work broadens our vision for the design of transition metal doped MoS_2 by synergetic optimization of the intrinsic HER kinetics and the active surface area for efficient hydrogen evolution.

ACKNOWLEDGEMENTS

We would like to acknowledge the financial supports from the National Natural Science Foundation of China (21501072，21706101 and 61674071), the Jiangsu Specially-Appointed Professors Program, the Natural Science Foundation of Jiangsu Province (BK20150489), the Opening Project of Key Laboratory of Green Chemistry of Sichuan Institutes of Higher Education (LZJ1702), the China Postdoctoral Science Foundation (2016M590419), the Jiangsu Province Postdoctoral Foundation (1501027A), and the Start Funding of Jiangsu University (15JDG011 and 15JDG027).

References

1. N.S. Lewis, D.G. Nocera, *Proc. Natl. Acad. Sci. U. S. A.*, 103 (2006) 15729.
2. J. Wang, H. Zhong, Z. Wang, F. Meng, X. Zhang, *ACS Nano*, 10 (2016) 2342.
3. S.S. Penner, *Energy*, 31 (2006) 33.
4. M. Wang, L. Chen, L. Sun, *Energy Environ. Sci.*, 5 (2012) 6763.
5. D. Yan, Y. Li, J. Huo, R. Chen, L. Dai, S. Wang, *Adv. Mater.*, 29 (2017) 1606459.
6. H.B. Gray, Nat. Chem., 1 (2009) 7.
7. X. Zhang, Z. Lai, C. Tan, H. Zhang, *Cheminform*, 47 (2016) 8816.
8. Y. Cheng, S. Lu, F. Liao, L. Liu, Y. Li, M. Shao, *Adv. Funct. Mater.*, 27 (2017) 1700359.
9. P. Chen, T. Zhou, M. Zhang, Y. Tong, C. Zhong, N. Zhang, L. Zhang, C. Wu, Y. Xie, *Adv. Mater.*, 29 (2017) 1701584.
10. W. Xiao, P. Liu, J. Zhang, W. Song, Y.P. Feng, D. Gao, J. Ding, *Adv. Energy Mater.*, 7 (2017) 1602086.
11. J.F. Callejas, C.G. Read, C.W. Roske, N.S. Lewis, R.E. Schaak, *Chem. Mater.*, 28 (2016) 6017.
12. Y. Shi, B. Zhang, *Chem. Soc. Rev.*, 45 (2016) 1781.
13. Z. Zhou, L. Wei, Y. Wang, H.E. Karahan, Z. Chen, Y. Lei, X. Chen, S. Zhai, X. Liao, Y. Chen, *J. Mate. Chem. A*, 5 (2017) 20390.
14. H. Duan, D. Li, Y. Tang, Y. He, J.S. Fang, R. Wang, H. Lv, P.P. Lopes, A.P. Paulikas, H. Li, *J. Am. Chem. Soc.*, 139 (2017) 5494.
15. K. Xu, D. Hui, M. Zhang, C. Min, Z. Hao, L. Zhang, C. Wu, X. Yi, *Adv. Mater.*, 29 (2017) 1606980.
16. J. Wang, F. Xu, H. Jin, Y. Chen, Y. Wang, *Adv. Mater.*, 29 (2017) 1605838.
17. B.W. Hao, Y.X. Bao, Y. Le, X.Y. Yu, W.L. Xiong, *Nat. Commun.*, 6 (2015) 6512.
18. J.S. Li, Y. Wang, C.H. Liu, S.L. Li, Y.G. Wang, L.Z. Dong, Z.H. Dai, Y.F. Li, Y.Q. Lan, *Nat. Commun.*, 7 (2016) 11204.
19. H. Lin, N. Liu, Z. Shi, Y. Guo, Y. Tang, Q. Gao, *Adv. Funct. Mater.*, 26 (2016) 5590.
20. W. Sheng, H.A. Gasteiger, S.H. Yang, *Acta Crystallogr.*, 157 (2010) B1529.
21. Y. Zheng, Y. Jiao, M. Jaroniec, S.Z. Qiao, *Angew. Chem.*, 54 (2015) 52.
22. L. Yang, W. Zhou, J. Lu, D. Hou, Y. Ke, G. Li, Z. Tang, X. Kang, S. Chen, *Nano Energy*, 22 (2016) 490.
23. J. Lai, S. Li, F. Wu, M. Saqib, R. Luque, G. Xu, *Energy Environ. Sci.*, 9 (2016) 1210.
24. Y. Li, H. Zhang, M. Jiang, Q. Zhang, P. He, X. Sun, *Adv. Funct. Mater.*, 27 (2017) 1702513.
25. A. Sivanantham, P. Ganesan, S. Shanmugam, *Adv. Funct. Mater.*, 26 (2016) 4661.

26. T. Liu, X. Ma, D. Liu, S. Hao, G. Du, Y. Ma, A.M. Asiri, X. Sun, L. Chen, *ACS Cataly.*, 7 (2017) 98.
27. Y. Feng, X.Y. Yu, U. Paik, *Chem. Commun.*, 52 (2016) 1633.
28. B. Mao, Q. Dong, Z. Xiao, C. Exstrom, S. Darveau, T. Webber, B. Lund, H. Huang, Z. Kang, J. Huang, *J. Mate. Chem. A*, 1 (2013) 12060.
29. J. Pan, C. Song, X. Wang, X. Yuan, Y. Fang, C. Guo, W. Zhao, F. Huang, *Inorg. Chem. Front.*, 4 (2017) 1895.
30. J. Staszakjirkovský, C.D. Malliakas, P.P. Lopes, N. Danilovic, S.S. Kota, K.C. Chang, B. Genorio, D. Strmcnik, V.R. Stamenkovic, M.G. Kanatzidis, *Nat. Mater.*, 15 (2016) 197.
31. J. Jiang, M. Gao, W. Sheng, Y. Yan, *Angew. Chem.*, 55 (2016) 15240.
32. Z. Wu, J. Guo, J. Wang, R. Liu, W. Xiao, C. Xuan, K. Xia, D. Wang, *ACS Appl. Mater. Interfaces*, 9 (2017) 5288.
33. T. An, Y. Wang, J. Tang, W. Wei, X. Cui, A.M. Alenizi, L. Zhang, G. Zheng, *J. Mate. Chem. A*, 4 (2016) 13439.
34. Y. Guo, L. Gan, C. Shang, E. Wang, J. Wang, *Adv. Funct. Mater.*, 27 (2017) 1602699.
35. B. Mao, Y. Yuan, Y. Shao, B. Yang, Z. Xiao, J. Huang, *Nanosci. Nanotech. Lett.*, 6 (2014) 685.
36. J. Huang, D. Hou, Y. Zhou, W. Zhou, G. Li, Z. Tang, L. Li, S. Chen, *J. Mate. Chem. A*, 3 (2015) 22886.
37. C. Wang, B. Ren, D. Li, Q. Jin, H. Cui, *J. Mate. Chem. A*, 5 (2017) 13196.
38. E. Atkins, *Phys. Today*, 10 (1978) 50.
39. M. Cabán-Acevedo, M.L. Stone, J.R. Schmidt, J.G. Thomas, Q. Ding, H.C. Chang, M.L. Tsai, J.H. He, S. Jin, *Nat. Mater.*, 14 (2015) 1245.
40. K. Chang, W. Chen, *ACS Nano*, 5 (2011) 4720.
41. G. Gong, Y. Liu, B. Mao, B. Wang, L. Tan, D. Li, W. Shi, *RSC Adv.*, 6 (2016) 99023.
42. X. Zheng, J. Xu, K. Yan, H. Wang, Z. Wang, S. Yang, *Chem. Mater.*, 26 (2014) 2344.
43. J. Huang, D. Hou, Y. Zhou, W. Zhou, G. Li, Z. Tang, L. Li, S. Chen, *J. Mate. Chem. A*, 3 (2015) 22886.
44. J. Miao, F.X. Xiao, H.B. Yang, Y.K. Si, J. Chen, Z. Fan, Y.Y. Hsu, H.M. Chen, H. Zhang, B. Liu, *Sci. Adv.*, 1 (2015) 1500259.
45. Y.J. Tang, Y. Wang, X.L. Wang, S.L. Li, W. Huang, L.Z. Dong, C.H. Liu, Y.F. Li, Y.Q. Lan, *Adv. Energy Mater.*, 6 (2016) 1600116.
46. Z. Wu, J. Guo, W. Jie, L. Rong, W. Xiao, C. Xuan, K. Xia, D. Wang, *ACS Appl. Mater. Interfaces*, 9 (2017) 5288.
47. J. Zhang, T. Wang, P. Liu, Z. Liao, S. Liu, X. Zhuang, M. Chen, E. Zschech, X. Feng, *Nat. Commun.*, 8 (2017) 15437.
48. Z. Pu, Q. Liu, A.M. Asiri, Y. Luo, X. Sun, Y. He, *Electrochim. Acta*, 168 (2015) 133.
49. Y. Liu, Q. Li, R. Si, G.D. Li, W. Li, D.P. Liu, D. Wang, L. Sun, Y. Zhang, X. Zou, Adv. Mater., 29 (2017) 1606200.
50. L.L. Feng, G. Yu, Y. Wu, G.D. Li, H. Li, Y. Sun, T. Asefa, W. Chen, X. Zou, *J. Am. Chem. Soc.*, 137 (2015) 14023.
51. P. Joo, K. Jo, G. Ahn, D. Voiry, Y.J. Hu, S. Ryu, M. Chhowalla, B.S. Kim, *Nano Lett.*, 14 (2014) 6456.
52. Y.Y. Chen, Y. Zhang, X. Zhang, T. Tang, H. Luo, S. Niu, Z.H. Dai, L.J. Wan, J.S. Hu, *Adv. Mater.*, 29 (2017) 1703311.
53. J. Zhang, T. Wang, P. Liu, Z. Liao, S. Liu, X. Zhuang, M. Chen, E. Zschech, X. Feng, *Nat. Commun.*, 8 (2017) 15437.
54. M. Fang, W. Gao, G. Dong, Z. Xia, S.P. Yip, Y. Qin, Y. Qu, J.C. Ho, *Nano Energy*, 27 (2016) 247.
55. X. Zou, Y. Zhang, *Chem. Soc. Rev.*, 44 (2015) 5148.
56. S. Wang, D. Yan, S. Dou, L. Tao, Z. Liu, Z. Liu, J. Huo, *J. Mate. Chem. A*, 4 (2016) 13726.
57. M.R. Gao, M.K.Y. Chan, Y. Sun, *Nat. Commun.*, 6 (2015) 7493.
58. R. Vellacheri, A. Al-Haddad, H. Zhao, W. Wang, C. Wang, Y. Lei, *Nano Energy*, 8 (2014) 231.

59. Z. Wang, D. Cao, L. Wen, R. Xu, M. Obergfell, Y. Mi, Z. Zhan, N. Nasori, J. Demsar, Y. Lei, *Nat. Commun.*, 7 (2016) 10348.
60. M.S. Faber, R. Dziedzic, M.A. Lukowski, N.S. Kaiser, Q. Ding, S. Jin, *J. Am. Chem. Soc.*, 136 (2014) 10053.
61. F. Li, L. Chen, G.P. Knowles, D.R. Macfarlane, J. Zhang, *Angew. Chem.*, 56 (2017) 505.